Available online at www.sciencedirect.com
SCIENCE DIRECT®
Journal of Sound and Vibration 273 (2004) 653–666
JOURNAL OF SOUND AND VIBRATION
www.elsevier.com/locate/jsvi

# Chaotic motion in the resonant separatrix bands of a Mathieu–Duffing oscillator with a twin-well potential

Albert C.J. Luo*

*Department of Mechanical and Industrial Engineering, Southern Illinois University at Edwardsville, Edwardsville, IL 62026-1805, USA*

Received 8 July 2002; accepted 30 April 2003

**Abstract**

The ($M$:1)-resonant bands in the left and right potential wells are skew-symmetric, and the ($2M$:1)-resonant bands of the large orbit motion are symmetric. The analytical conditions for the onset and destruction of a resonant band are developed through the incremental energy approach. The numerical predictions of such onset and destruction are also completed by the energy increment spectrum method. The sub-resonance interaction occurs for strong excitations, which needs to be further investigated. These results are applicable to the small- and large-orbit motions of post-buckled structure under a parametric excitation.


## 1. Introduction

Consider a Mathieu–Duffing oscillator with a twin-well potential,

$$\ddot{x} - [\alpha_1 + Q_0 \cos(\Omega t)]x + \alpha_2 x^3 = 0, \tag{1}$$

where system parameters $\alpha_1 > 0$ and $\alpha_2 > 0$ are relative to linear and non-linear terms in the equations of motion for buckled structures. The longitudinal loading is periodic, and $Q_0$ and $\Omega$ are the excitation strength and frequency of the periodic loading, respectively. For weak excitations, Yamaguchi [1] in 1985 investigated the structure of stochastic layer for such an oscillator through the Chirikov overlap presented in Ref. [2]. The chaotic motion in the vicinity of generic separatrix (i.e., stochastic layer or the generic separatrix band) for such an oscillator is

*Tel.: +1-618-650-5389; fax: +1-618-650-2555.
*E-mail address:* aluo@siue.edu (A.C.J. Luo).

0022-460X/03/$ - see front matter 
doi:10.1016/S0022-460X(03)00564-9

investigated [3]. It was found that the resonance embedded in the generic separatrix band was different from what the traditional analysis gives. For a clear understanding of the resonant dynamics of chaotic motion in such an oscillator, the chaotic motion in the vicinity of a specified, resonant separatrix band will be of great interest.

In 1868, Mathieu [4] for at the first time investigated the linear Mathieu equation (also see Refs. [5,6]). In 1913, Whittaker [7] developed an approach to find the unstable solution for very weak excitation (also see Ref. [8]). In addition, other contributions to the solutions of the Mathieu equations can be found (e.g., Ref. [9]). The aforementioned investigations were based on the purely mathematical discussion. However, in engineering, Sevin [10] investigated the parametric excitation of a pendulum-type vibration absorber via the linear Mathieu equation in 1961. In 1965, Hsu [11] developed the first-approximation analysis and instability criteria for a parametrically excited, linear system with multiple degrees of freedom, and further results were presented in Ref. [12]. In 1965, Tso and Caughey [13] investigated the parametric vibration of a non-linear system through the slowly varying parameter technique, and in 1993, Mond et al. [14] investigated the stability analysis of non-linear Mathieu equation though the normal form technique. Such a technique cannot provide quantitative predictions of chaotic motions in parametric oscillators. The quasi-periodic Mathieu oscillators were also investigated in Ref. [15].

In 1962, Melnikov [16] discussed the resonant motion in the resonant separatrix based on the perturbation analysis (also see Ref. [17]). In 1964, the chaotic motion in the vicinity of resonant separatrix was observed by Henon and Heiles [18] through the numerical simulation of the internal resonant layer in a two-degrees of freedom, non-linear system. In 1979, Chirikov [2] investigated such a problem through the whisker map, and the Chirikov resonance overlap criterion was proposed. Based on the Chirikov's concept, in 1981, Escande and Doveil [19] developed the renormalization group scheme to determine the overlap of two resonant bands, and the detailed discussion was presented in Ref. [20]. In 1992, Lichtenberg and Lieberman [21] gave the qualitative description of chaotic motions in the resonant layer (or band). Because it is difficult to determine the location of the resonant separatrix, it seemed that the analytical and numerical predictions of the forming and destruction of resonant layers were impossible. In 1995, Luo [22] proposed an analytical approach (i.e., the incremental energy approach) to determine the onset of the resonant layer in non-linear Hamiltonian systems with periodic excitations (also see Ref. [23]). In 1999, Luo and Han [24] modified the Chirikov overlap approach to investigate the chaotic motion in resonant bands, and the corresponding criteria for the resonant overlap were given. The two analytical methods are based on the certain approximation assumptions. To verify the two approaches, in 2002, Luo [25] developed an energy increment spectrum method to numerically predict the onset and disappearance of the resonant bands, and such an approach was applied to the parametrically excited pendulum. Since the Mathieu–Duffing oscillator is extensively used for parametric non-linear vibrations in engineering, it is important to better understand its non-linear dynamical characteristics. To extend work in Ref. [3], herein, the chaotic motion in the primary resonance band will be investigated.

In this paper, the approximate criteria for the onset and destruction of a specified, primary resonant band of the Mathieu–Duffing oscillator will be developed. The numerical investigation on the appearance and disappearance of the specified primary resonant band will be completed. Numerical simulations will be carried out for illustration of the resonant bands in the Mathieu–Duffing oscillator.

## 2. Energy analysis and resonance

The total energy for Eq. (1) is $H = H_0 + H_1$, where the time-independent $H_0$ (unperturbed) and time-dependent $H_1$ (perturbation) in the Hamiltonian of Eq. (1) are

$$H_0 = \tfrac{1}{2}\dot{x}^2 - \tfrac{1}{2}\alpha_1 x^2 + \tfrac{1}{4}\alpha_2 x^4, \quad H_1 = -\tfrac{1}{2}x^2 Q_0 \cos(\Omega t). \tag{2}$$

The unperturbed system of Eq. (1) possesses a homoclinic separatrix related to the saddle point $(0,0)$ for $H_0 = E_0 = 0$. This separatrix separates the motions of the unperturbed Duffing oscillator into large and small orbit motions. The small orbit motion is in one of the two potential wells, and the large orbit motion is located outside the two potential wells. Hence, under a periodic excitation, the resonance for the two motions will occur. For enough strong excitations, the resonant separatrix will be developed. Furthermore, the chaotic motions in the vicinity of such a resonant separatrix associated with small and large orbit motion are investigated.

### 2.1. Small orbit motion

For a given energy $H_0 = E_s < E_0 = 0$, the solution of the small orbit motion without the excitation in Refs. [3,22] is

$$x_s^0 = \pm e_s \,\mathrm{dn}\left[\frac{K(k_s)\omega_s t}{\pi}, k_s\right], \tag{3}$$

where dn is the Jacobi–elliptic function, $K(k)$ the complete elliptic integral of the first kind and $k$ the modulus of the Jacobi–elliptic function, and the subscript $s$ denotes the small orbit. The modulus $k_s$, the response amplitude $e_s$ and the natural frequency $\omega_s$ are

$$k_s = \sqrt{\frac{2\sqrt{\alpha_1^2 + 4\alpha_2 E_s}}{\alpha_1 + \sqrt{\alpha_1^2 + 4\alpha_2 E_s}}}, \quad e_s = \sqrt{\frac{2\alpha_1}{(2 - k_\alpha^2)\alpha_2}}, \quad \omega_s = \frac{\sqrt{\alpha_2}e_s\pi}{\sqrt{2}K(k_s)}. \tag{4}$$

As the unperturbed solution in Eq. (3) is used to approximate the perturbed one, the total energy is approximated by

$$H = H_0(x,y) - \tfrac{1}{2}x^2 Q_0 \cos(\Omega t) \approx E_s - \tfrac{1}{2}(x_s^0)^2 Q_0 \cos(\Omega t). \tag{5}$$

To show how to obtain the foregoing approximation, consider a small perturbation excitation (i.e., $Q_0 \sim \varepsilon$): a perturbed solution ($x = x_0 + \varepsilon x_1 + \cdots$) is inserted in the middle part of Eq. (5) and the higher order ($\varepsilon^n, n \geqslant 2$) perturbation terms are dropped. Further, the last part of Eq. (5) is obtained. As in Refs. [22,24], substitution of Eq. (3) into Eq. (5) and a Fourier expansion of the time-dependent term gives

$$H \approx E_s - \frac{\pi^2 e_s^2 Q_0}{4K^2}\left\{\frac{1}{2}\cos\Omega t + \sum_{M=1}^{\infty}\left[p_M + \frac{1}{2}\sum_{m=1}^{\infty}\sum_{n=1}^{\infty}(p_m p_n \delta_{m+n}^M + p_m p_n \delta_{|m-n|}^M)\right] \times [\cos(M\omega_s - \Omega)t + \cos(M\omega_s + \Omega)t]\right\}, \tag{6}$$

where

$$p_m = \operatorname{sech}\left[\frac{m\pi K'}{K}\right] \quad \text{and} \quad K'(k_s) = K(k_s'), \quad k_s' = \sqrt{1-k_s^2}. \tag{7}$$

From the averaging of the Hamiltonians in Eq. (6), $\bar{H} = \frac{1}{T}\int_0^T H(x,y,t)\,\mathrm{d}t$ should be bounded, which gives the resonant condition (as in Ref. [21]) as

$$M\omega_s = \Omega \quad \text{and} \quad M = \{m+n, |m-n|\}. \tag{8}$$

Note that the resonance relative to $p\omega = q\Omega$ is termed the ($p$:$q$) resonance. Therefore, in the small orbit motion, the ($M$:1)-resonant motion exists.

### 2.2. Large orbit motion

In a similar fashion, for $H_0 = E_l > E_0 = 0$, the solution of the large orbit motion [3,22] is

$$x_l^0 = e_l \operatorname{cn}\left[\frac{2K(k_l)\omega_l t}{\pi}, k_l\right]. \tag{9}$$

The modulus $k_l$, the response amplitude $e_l$, and the natural frequency $\omega_l$ are

$$k_l = \sqrt{\frac{\alpha_1 + \sqrt{\alpha_1^2 + 4\alpha_2 E_l}}{2\sqrt{\alpha_1^2 + 4\alpha_2 E_l}}}, \quad e_l = \sqrt{\frac{2k_l^2\alpha_1}{(2k_l^2-1)\alpha_2}}, \quad \omega_l = \frac{\sqrt{\alpha_2}e_l\pi}{2\sqrt{2}k_l K(k_l)}. \tag{10}$$

Use of the unperturbed solution in Eq. (9) as a perturbed one and a Fourier expansion of the time-dependent term in the total energy gives

$$\begin{aligned} H &\approx E_l - \frac{1}{2}(x_l^0)^2 Q_0 \cos(\Omega t) \\ &= E_l - \frac{\pi^2 e_l^2 Q_0}{8k_l^2 K^2} \sum_{M=1}^{\infty}\sum_{m=1}^{\infty}\sum_{n=1}^{\infty} (q_{2m-1}q_{2n-1}\delta^{2M}_{2(m+n-1)} + q_{2m-1}q_{2n-1}\delta^{2M}_{2|m-n|}) \\ &\quad \times [\cos(2M\omega_l - \Omega)t + \cos(2M\omega_l + \Omega)t], \end{aligned} \tag{11}$$

where

$$q_m = \operatorname{sech}\left[\left(m - \frac{1}{2}\right)\frac{\pi K'}{K}\right] \quad \text{and} \quad K'(k_l) = K(k_l'), \quad k_l' = \sqrt{1-k_l^2}. \tag{12}$$

In an alike manner, from Eq. (11), the bounded averaging of the Hamiltonians gives the resonant condition (as in Ref. [21]):

$$2M\omega_l = \Omega \quad \text{and} \quad M = \{m+n-1, |m-n|\}. \tag{13}$$

From traditional analysis (e.g., linearization and perturbation or normal form), the resonant condition in potential wells should be ($2M$:1) and outside potential wells it should be ($2(2M-1)$:1). However, based on the above energy analysis, the resonant conditions for the two cases become ($M$:1) and ($2M$:1). Especially, the resonant conditions in the two potential wells of the Mathieu–Duffing oscillator are the same as in the two potential wells of the forced Duffing oscillator in Refs. [22–24]. That is why resonant conditions for non-linear dynamic systems

hindered one to investigate the resonant motions. Therefore, one just assumed a resonant condition (e.g., (1:1) or (2:1)) based on intuitive observation to analyze the corresponding dynamic behaviors through such as perturbation, linearization, normal form, etc. From a literature survey, it can be found that the assumed resonant conditions for internal resonance are very popular, which may not be a proper way to work out resonant motions in non-linear systems (also see Ref. [2]).

## 3. Energy increment spectrum

Luo [25] developed an energy increment spectrum approach for the numerical prediction of the onset and disappearance of the resonant band (or the resonant separatrix band). Such an energy increment spectrum approach is used for determining the critical value of excitation frequency for a given excitation strength. This energy increment spectrum is based on the energy of the Poincaré mapping points of the separatrix band. The Poincaré mapping points for the twin-well Duffing oscillator are defined through the section:

$$\Sigma = \left\{ (x(t_N), \dot{x}(t_N)) | \text{ satisfying Eq. (1), and } t_N = \frac{2N\pi}{\Omega} + t_0, N = 0, 1, \ldots \right\}, \tag{14}$$

where $x(t_N) = x_N$, $\dot{x}(t_N) = \dot{x}_N$ and the initial conditions are $x(t_0) = x_0$, $\dot{x}(t_0) = \dot{x}_0$ at $t = t_0$. The Poincaré map is $P{:}\Sigma \to \Sigma$. The energy for each Poincaré mapping point of the Duffing oscillator for iteration time $N$ is computed through

$$H_0^{(N)} = \tfrac{1}{2}\dot{x}_N^2 - \tfrac{1}{2}\alpha_1 x_N^2 + \tfrac{1}{4}\alpha_2 x_N^4, \tag{15}$$

and the corresponding minimum and maximum energy increments are defined through

$$\Delta E_{\max} = \max_{N\to\infty}\{H_0^{(N)} - E_s^{(M:1)}\} \quad \text{and} \quad \Delta E_{\min} = \min_{N\to\infty}\{H_0^{(N)} - E_s^{(M:1)}\} \tag{16}$$

for the $(M{:}1)$-resonance relative to the small orbit motion, and

$$\Delta E_{\max} = \max_{N\to\infty}\{H_0^{(N)} - E_l^{(2M:1)}\} \quad \text{and} \quad \Delta E_{\min} = \min_{N\to\infty}\{H_0^{(N)} - E_l^{(2M:1)}\} \tag{17}$$

for the $(2M{:}1)$-resonance relative to the large orbit motion.

Herein, the resonant energies $E_s^{(M:1)}$ (or $E_l^{(2M:1)}$) are computed through the corresponding resonant conditions. Namely, once an excitation frequency $\Omega$ is given, the resonant condition in Eq. (8) (or Eq. (13)) gives the natural frequency $\omega_s$ (or $\omega_l$). Furthermore, the resonant energy $E_s^{(M:1)}$ (or $E_l^{(2M:1)}$) is computed by use of Eq. (4) (or Eq. (10)). From the foregoing definitions, the maximum and minimum energy increment spectra are computed through a second order symplectic scheme in Refs. [26,27] with time step $\Delta t = 10^{-6} \sim 10^{-7}T$, where $T = 2\pi/\Omega$, and with a precision of $10^{-8}$. Consider the parameter $\alpha_1 = \alpha_2 = 1.0$ in Eq. (1). Theoretically, exact critical values for the appearance and disappearance of a specified resonant separatrix band should be obtained as $N \to \infty$. With increasing finite iteration numbers, the computational results of critical values are much closer to the exact values. Note that the energy increment extrema in Eqs. (16) and (17) are relative values for specified finite iteration numbers. From numerical simulation experimentations, the critical results with a relative error of 1% are acceptable for 1000-periods of iterations, compared to $10^6$-periods of iteration. For 10 000-periods of iterations, the relative error

percentages of the critical values of excitation frequency are less than 0.1%. Therefore, the maximum and minimum energy increments are computed from 10 000 iterations of the Poincaré map for each excitation frequency instead of infinite iterations. In the two plots of Fig. 2, $\Omega^{app}$ and $\Omega^{dis}$ denote excitation frequencies for the appearance and disappearance of the resonant bands. In Fig. 1(a), the appearance and disappearance frequencies $\Omega_s^{app(2:1)} \approx 2.2332655020$ and $\Omega_s^{dis(2:1)} \approx 2.1057711710$. For the appearance of the (2:1)-resonant band, the minimum energy increment drops suddenly with a large jump to a negative value. However, the disappearance of the resonant band makes the maximum energy increment jump suddenly up to a positive value.

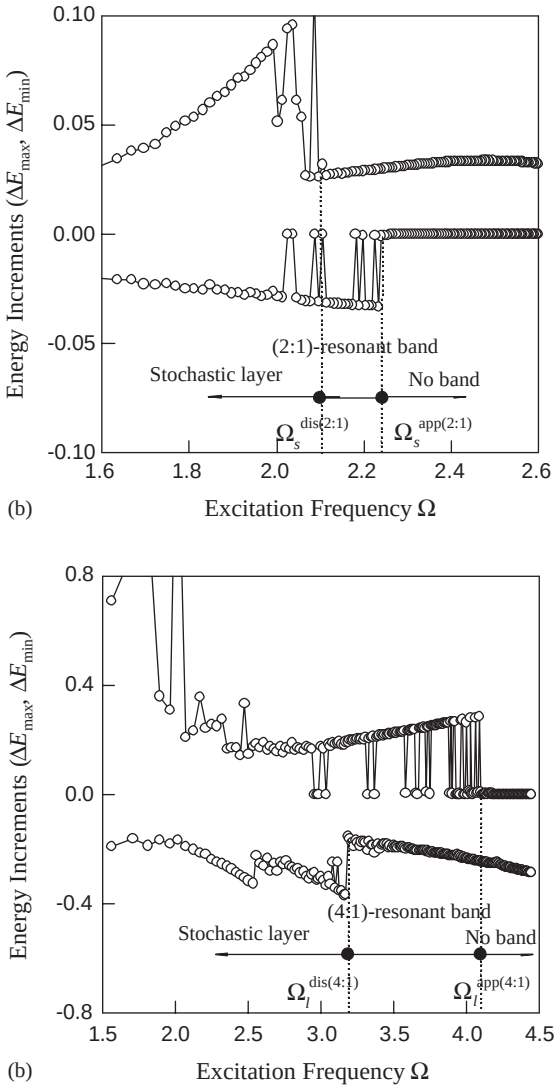


Fig. 1. Maximum and minimum energy increment spectrums ($\alpha_1 = \alpha_2 = 1$) for (a) the (2:1)-resonant band relative to the small orbit motion ($Q_0 = 0.01$), and (b) the (4:1)-resonant band relative to the large orbit motion ($Q_0 = 0.1$).

The maximum energy of the resonant band increases to the higher order resonant energy. For $\Omega > \Omega_s^{dis(2:1)}$, the minimum energy increment almost is zero. It indicates that the resonant separatrix cannot be formed. Such a frequency range is termed the non-resonant band zone. At $\Omega = \Omega_s^{dis(2:1)}$, the maximum energy increment jumps to the higher energy level very close to the homoclinic orbit energy level, and the (2:1)-resonant band relative to the small orbit motion is destroyed. Furthermore, the stochastic layer appears. The chaotic motion will be generated by the overlap between the stochastic layer and resonant band. Similarly, the energy increment spectrum for the (4:1)-resonant band relative to the large orbit motion is illustrated in Fig. 1(b). We have the two critical values $\Omega_l^{app(4:1)} \approx 2.448938644$ and $\Omega_l^{dis(4:1)} \approx 2.213713491$. For the appearance of the (4:1)-resonant band pertaining to the large orbit motion, the maximum energy increment jumps to a new positive value, but the disappearance of the resonant band makes the minimum energy increment drop to a negative value.

## 4. Approximate criteria

### 4.1. Small orbit motion

To develop analytical conditions, an energy increment along the inner $(M{:}1)$-resonant orbit in the two-wells needs to be computed. Such an energy increment is approximated by

$$\begin{aligned}\Delta H_0^s(\varphi_i) &= 2\int_{t_i}^{T_s+t_i} [H_0, H_1]\,\mathrm{d}t = 2\int_{t_i}^{T_s+t_i} (f_1 g_2 - f_2 g_1)\,\mathrm{d}t \\ &\approx 2\int_{t_i}^{T_s+t_i} x_\alpha^{(0)} y_\alpha^{(0)} Q_0 \cos(\Omega t)\,\mathrm{d}t = 2Q_0 Q_s^{(M:1)} \sin\varphi_i, \end{aligned} \tag{18}$$

where $\varphi_i = \Omega t_i$, $[\cdot, \cdot]$ is the Poisson bract and

$$\begin{aligned} &f_1 = y = \dot{x}, \quad g_1 = \alpha_1 x - \alpha_2 x^3, \\ &f_2 = 0, \quad g_2 = x Q_0 \cos\Omega t; \end{aligned} \tag{19}$$

$$Q_s^{(M:1)} = \frac{\pi^2 \Omega}{K\alpha_2}\sqrt{\frac{\alpha_1}{2-k^2}}\left[p_M + \frac{1}{2}\sum_{m=1}^{\infty}\sum_{n=1}^{\infty}(p_m p_n \delta_{m+n}^M + p_m p_n \delta_{|m-n|}^M)\right]. \tag{20}$$

The above integration is completed through the Fourier series expansion combined with the $(M{:}1)$-resonant condition.

From Eq. (4), the phase change under one period $(T_s = 2\pi/\omega_s)$ is computed by

$$\Delta\varphi^s(E_s) = \frac{2\pi\Omega}{\omega_s} = \frac{2\Omega\sqrt{2-k_s^2}K(k_s)}{\sqrt{\alpha_1}}. \tag{21}$$

Therefore, from the energy change in Eq. (18), $\Delta H_0^s = E_s^{(i+1)} - E_s^{(i)}$, and the phase change $\Delta\varphi = \varphi_{i+1} - \varphi_i$ for one period $T_s$, the accurate whisker map for the $(M{:}1)$-resonant band of the

Mathieu–Duffing oscillator is

$$E_s^{(i+1)} - E_s^{(i)} \approx 2Q_0 Q_s^{(M:1)} \sin\varphi_i, \quad \text{and} \quad \varphi_{i+1} - \varphi_i = \frac{2\pi\Omega}{\omega_s} = \frac{2\Omega\sqrt{2-(k_s)^2}K(k_s)}{\sqrt{\alpha_1}}. \tag{22}$$

For the $(M{:}1)$-resonant band, we assume $\varphi_{i+1} - \varphi_i = \varphi_{i+1}^{(M:1)} - \varphi_i^{(M:1)} = 2M\pi$ to satisfy the $(M{:}1)$-resonant condition in Eq. (18). From the second of Eqs. (22), the modulus $k_s^{(M:1)}$ can be computed, and from which $E_s^{(M:1)}$ can be obtained. If $E_s^{(i+1)} = E_s^{(i)} = E_s^{(M:1)}$, the first equation of Eqs. (22) gives $\varphi_i^{(M:1)} = 0, \pi$. As in Ref. [21], using the energy and phase relative to the $(M{:}1)$-resonance leads to a standard map if $w_i = (E_s^{(i+1)} - E_s^{(M:1)})G_s^{(M:1)}$ and $\phi_i = \varphi_i - \varphi_i^{(M:1)}$, i.e.,

$$w_{i+1} = w_i + B\sin\phi_i \quad \text{and} \quad \phi_{i+1} \approx \phi_i + w_{i+1}, \tag{23}$$

where $G_s^{(M:1)}\Delta H_0^s(\varphi_i) = B\sin\phi_i$ and $G_s^{(M:1)} = \partial(2\pi\Omega/\omega_s)/\partial E_i|_{E_s^{(M:1)}}$. For the foregoing, the strength of the stochasticity parameter is $B = B^* \approx 0.9716\cdots$ in Refs. [28,29] for the transition to global stochasticity in Eq. (23). Therefore, the excitation strength for the onset of a resonant band is approximated by

$$Q_0 \approx \frac{0.4858}{Q_s^{(M:1)} G_s^{(M:1)}}, \tag{24}$$

where

$$G_s^{(M:1)} = -\frac{\Omega\alpha_2[2-(k_s^{(M:1)})^2]^{5/2}}{(k_s^{(M:1)})^4\alpha_1^2\sqrt{\alpha_1}}\left\{2K(k_s^{(M:1)}) - \frac{2-(k_s^{(M:1)})^2}{1-(k_s^{(M:1)})^2}E(k_s^{(M:1)})\right\}. \tag{25}$$

As in Refs. [22,23], from Eq. (18), the incremental energy approach gives the approximate criteria for destruction of the resonant separatrix band, i.e.,

$$Q_0 = \min\frac{1}{2Q_s^{(M:1)}}\{|E_s^{(M:1)} - E_s^{(M-1:1)}|, |E_s^{(M:1)} - E_s^{(M+1:1)}|\}. \tag{26}$$

### 4.2. Large orbit motion

In a similar fashion, the energy increment for the $(2M{:}1)$-resonant band under one period $(T_l = 2\pi/\omega_l)$ is

$$\Delta H_0^l(\varphi_i) = \int_{t_i}^{T_l+t_i}[H_0, H_1]\,\mathrm{d}t \approx \int_{t_i}^{T_l+t_i} x_l^{(0)} y_l^{(0)} Q_0\cos(\Omega t)\,\mathrm{d}t = Q_0 Q_l^{(2M:1)}\sin\varphi_i \tag{27}$$

and

$$Q_l^{(2M:1)} = \frac{\pi^2\Omega}{K\alpha_2}\sqrt{\frac{\alpha_1}{2k_l^2-1}}\sum_{m=1}^{\infty}\sum_{n=1}^{\infty}(q_{2m-1}q_{2n-1}\delta^{2M}_{2(m+n-1)} + q_{2m-1}q_{2n-1}\delta^{2M}_{2|m-n|}). \tag{28}$$

The phase change under one period $(T_l = 2\pi/\omega_l)$ from Eq. (10) is

$$\Delta\varphi^l(E_l) = \frac{2\pi\Omega}{\omega_l} = \frac{4\Omega K(k_l)\sqrt{2k_l^2-1}}{\sqrt{\alpha_1}}. \tag{29}$$

Therefore, from Eq. (27) and phase change, the accurate whisker map for the $(2M{:}1)$-resonant band of the Mathieu–Duffing oscillator is

$$E_l^{(i+1)} - E_l^{(i)} \approx Q_0 Q_l^{(2M:1)} \sin\varphi_i, \quad \varphi_{i+1} - \varphi_i = \frac{2\pi\Omega}{\omega_l} = \frac{4\Omega\sqrt{2(k_l)^2 - 1}K(k_l)}{\sqrt{\alpha_1}}. \tag{30}$$

The excitation strength for the onset of the $(2M{:}1)$-resonant band is

$$Q_0 \approx \frac{0.9716}{Q_l^{(2M:1)} G_l^{(2M:1)}}, \tag{31}$$

where

$$\mathrm{G}_l^{(2M:1)} = -\frac{2\Omega\alpha_2[2(k_l^{(2M:1)})^2 - 1]^{5/2}}{(k_l^{(2M:1)})^2\alpha_1^2\sqrt{\alpha_1}}\left[K(k_l^{(2M:1)}) - \frac{1 - 2(k_l^{(2M:1)})^2}{1 - (k_l^{(2M:1)})^2}E(k_l^{(2M:1)})\right]. \tag{32}$$

The approximate condition for the disappearance of the $(2M{:}1)$-resonant band is

$$Q_0 = \min\frac{1}{Q_l^{(2M:1)}}\{|E_l^{(2M:1)} - E_l^{(2M-2:1)}|, |E_l^{(2M:1)} - E_l^{(2M+2:1)}|\}. \tag{29'}$$

### 4.3. Illustrations

The numerical and analytical predictions of excitation strengths for the onset and disappearance of a specified resonant band for the Mathieu–Duffing oscillators are presented in Fig. 2. The solid and dashed curves denote the analytical conditions for the onset and destruction of the resonant band, respectively. The solid and hollow circular symbol curves represent the numerical predictions of the onset and destruction of the resonant bands, respectively. In Fig. 2(a), it is observed that the agreement between the two predictions is not very good for the lower-order resonance partially because the unperturbed solution is used to obtain the approximate analytical condition and partially because the sub-resonance is not considered. It is very difficult to obtain the (5:1)-order and higher resonant bands by numerical predictions since they are too close to the homoclinic orbit. For large orbit resonant bands, the two predictions do not agree very well, as shown in Fig. 2(b). For strong excitations, the frequency ranges of the resonant band become wider with a catastrophe. This is because a new sub-resonant web is strongly involved in the resonant band. The sub-resonance influence on the large orbit resonant motion is much stronger than on the small orbit resonant motion. For such a phenomenon, the further mathematical model including the sub-resonance structures should be developed. For the (2:1)-resonant band, it is very difficult to detect through the numerical prediction. Before such a resonant band is formed, the sub-resonant webs already cause the resonant band to be destroyed and the stochastic layer is formed for such a Mathieu–Duffing oscillator. For a given excitation frequency, multi-values of excitation strength can be observed because the different-order resonant motion can be induced by different excitation strengths with different initial conditions (also see Ref. [24]).

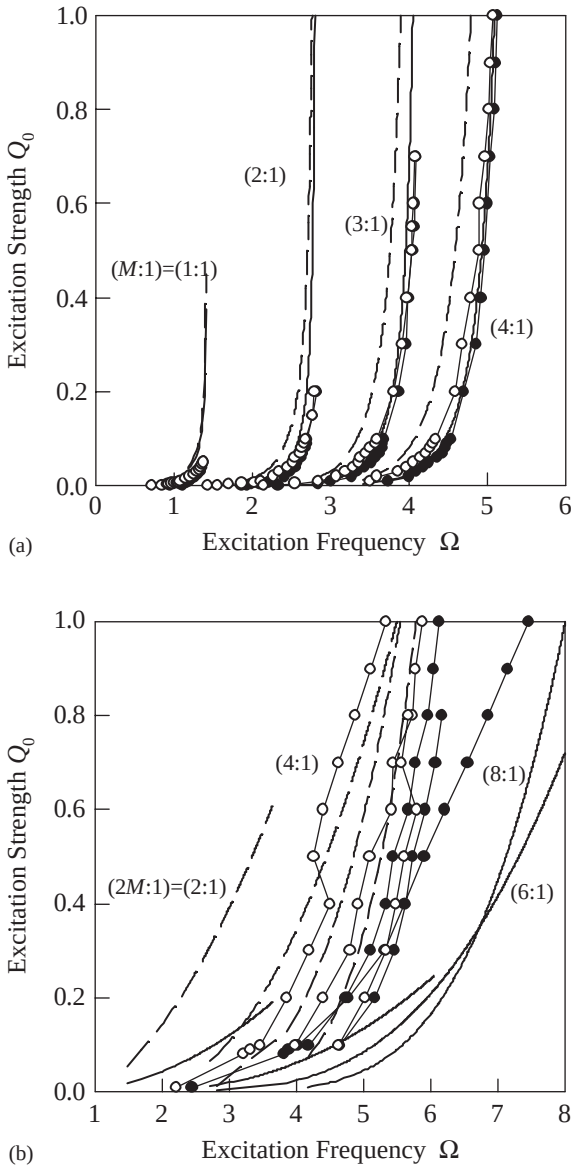


Fig. 2. Analytical and numerical predictions of excitation strength for resonant bands relative to (a) the small orbit motion in the potential wells, and (b) the large orbit motion outside the potential wells ($\alpha_1 = \alpha_2 = 1$). The solid and dashed curves denote the analytical conditions for the onset and destruction of the resonant band, respectively. The solid and hollow circular symbol curves represent the numerical predictions of the onset and destruction of the resonant bands, respectively.

## 5. Numerical demonstrations

In this section, the resonant bands of the Mathieu–Duffing oscillator with a twin-well potential are demonstrated for a better understanding of the resonant band dynamics. The resonant bands

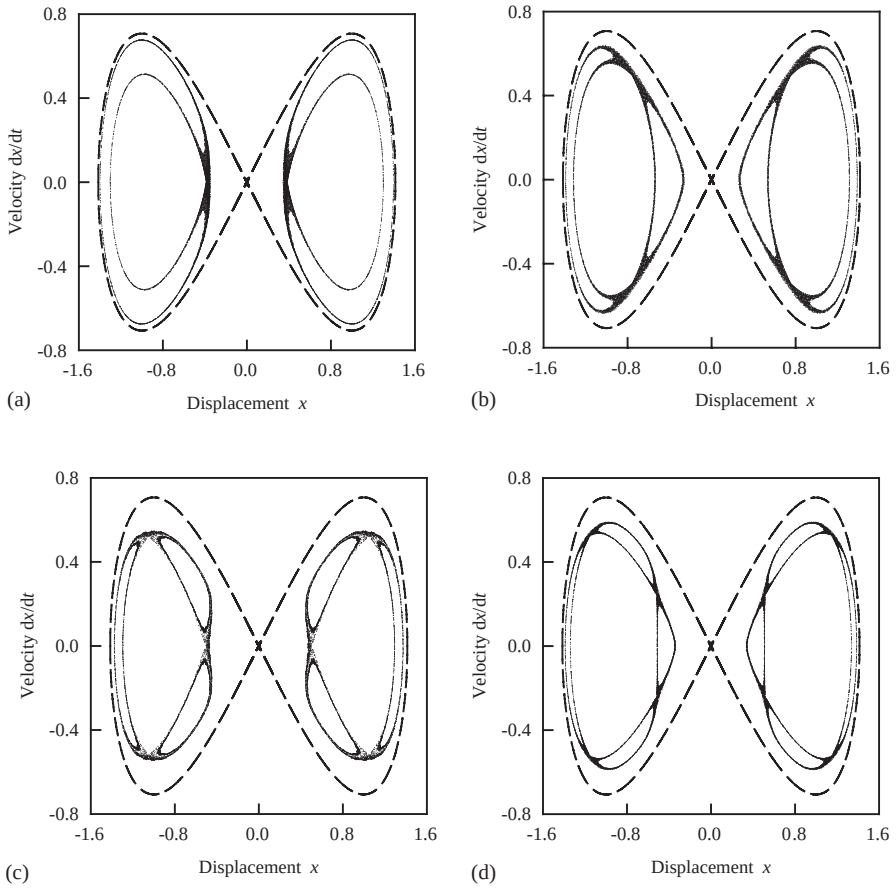


Fig. 3. Poincaré mapping sections for resonant bands in potential wells: (a) (1:1)-resonant band ($\Omega = 1.123544342$, $x_0 = \pm 0.3815751898$, $\mathrm{d}x_0/\mathrm{d}t = 0.$, $Q_0 = 0.01$), (b) (2:1)-resonant band ($\Omega = 2.298928874$, $x_0 = \pm 0.7461745158$, $\mathrm{d}x_0/\mathrm{d}t = \pm 0.4967659648$, $Q_0 = 0.02$), (c) (3:1)-resonant band ($\Omega = 3.652117934$, $x_0 = \pm 1.033192846$, $\mathrm{d}x_0/\mathrm{d}t = \pm 0.5293606725$, $Q_0 = 0.1$), (d) (4:1)-resonant band ($\Omega = 4.657816650$, $x_0 = \pm 1.1338433810$, $\mathrm{d}x_0/\mathrm{d}t = \pm 0.5401074783$, $Q_0 = 0.2$). The dashed curve is the homoclinic orbit.

associated with the small and large orbit motions are illustrated through the Poincare mapping sections in Figs. 3 and 4, respectively. The (1:1)-resonant band is simulated with the initial condition ($x_0 = \pm 0.3815751898$ and $\mathrm{d}x_0/\mathrm{d}t = 0.$) and excitation frequency and strength ($\Omega = 1.123544342$ and $Q_0 = 0.01$), as shown in Fig. 3(a). The (1:1)-resonant bands in the left and right wells are symmetric (also skew-symmetric). Their dynamic behaviors will be identical. In Fig. 3(b), we consider $Q_0 = 0.02$ rather than $Q_0 = 0.01$ since for such excitation strength, the (2:1)-resonant band is very thin, and the excitation frequency $\Omega = 2.298928874$ is used as well. To make the resonant band identical, the corresponding initial conditions for the left and right wells are $x_0 = \pm 0.7461745158$ and $\mathrm{d}x_0/\mathrm{d}t = \pm 0.4967659648$. Since the motion orbit is always clockwise, the (2:1)-resonant bands between the left and right wells are skew-symmetric. This characteristics for all the ($M$:1)-resonant band of the orders higher than 1 (i.e., $M > 1$ ) should

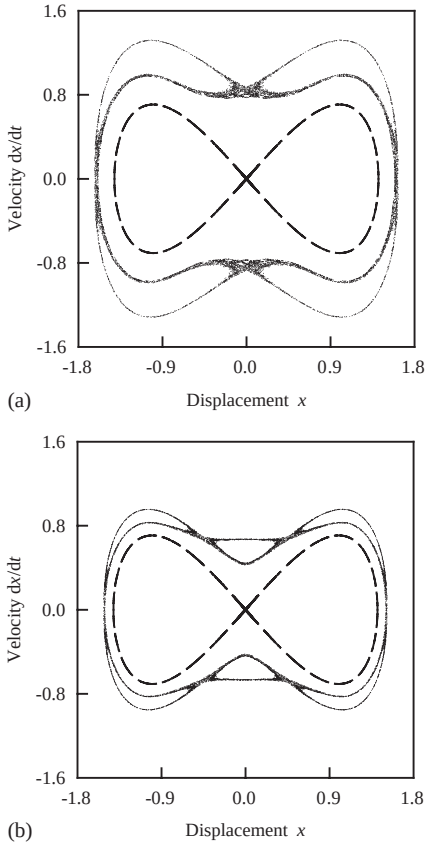


Fig. 4. Poincaré mapping sections for resonant bands relative to the large motion ($Q_0 = 0.1$): (a) (4:1)-resonant band ($\Omega = 3.498195658$, $x_0 = 1.6163080040$, $dx_0/dt = 0.$), (b) (6:1)-resonant band ($\Omega = 4.176975085$, $x_0 = 1.507578257$, $dx_0/dt = 0.$). The dashed curve is the homoclinic orbit.

exist. To further observe the higher order resonant bands, the (3:1)-resonant band with parameters and initial conditions ($\Omega = 3.652117934$, $Q_0 = 0.1$ and $x_0 = \pm 1.033192846$, $dx_0/dt = \pm 0.5293606725$) are computed, as shown in Fig. 3(c), and the (4:1)-resonant band is simulated for parameters and initial conditions ($\Omega = 4.657816650$, $Q_0 = 0.2$ and $x_0 = \pm 1.1338433810$, $dx_0/dt = \pm 0.5401074783$) in Fig. 3(d). The resonant band plots show the resonant band features for different resonance orders. The island domains formed by the resonant separatrix are the maximum resonant attractive domains once the damping is considered in such a Mathieu–Duffing oscillator. Such an issue will be discussed in sequel. From the previous analysis, the resonant bands relative to the small and large orbit motions are different, only the even order resonant bands outside the potential wells exist. To demonstrate the even order resonant bands, the (4:1)- and (6:1)-resonant bands are presented in Fig. 4 for $Q_0 = 0.1$. For the (4:1)-resonant band, we consider the excitation frequency ($\Omega = 3.498195658$) with the corresponding initial conditions ($x_0 = 1.6163080040$ and $dx_0/dt = 0.$), as shown in Fig. 4(a). The resonant band is symmetric, namely, the hyperbolic and parabolic points and the sub-resonance are distributed in

Poincare mapping sections. For the same excitation strength, the (6:1)-resonant band is computed for the excitation frequency ($\Omega = 4.176975085$) and the initial condition ($x_0 = 1.507578257$ and $dx_0/dt = 0.$). It is observed that the (6:1)-resonant band is much closer to the homoclinic orbit than the (4:1)-resonant band, and the bandwidth becomes much smaller. With increasing the resonant order, the resonant separatrix bandwidth will decrease.

## 6. Conclusion

The dynamic characteristics of the ($M$:1)- and ($2M$:1)-resonant bands for the inside and outside of the homoclinic orbit of the Mathieu–Duffing oscillator are investigated. The ($M$:1)-resonant bands in the left and right potential wells are skew-symmetric. The (2M:1)-resonant band structure of the large orbit motion are symmetric in the Poincare mapping section. As the excitation becomes strong, the analytical and numerical predictions for such (2M:1)-resonant bands do not match each other well due to the approximate computation of the energy increment and sub-resonance effects. When the excitation strength increase to some values, the sub-resonance interaction occurs, which needs to be further investigated.

## References

[1] Y. Yamaguchi, Structure of the stochastic layer of a perturbed double-well potential system, *Physics Letters A* 109 (5) (1985) 191–195.
[2] B.V. Chirikov, A universal instability of many-dimensional oscillator systems, *Physics Report* 52 (1979) 263–379.
[3] A.C.J. Luo, Chaotic motion in the generic separatrix band of a Mathieu–Duffing oscillator with a twin-well potential, *Journal of Sound and Vibration* 248 (3) (2001) 521–532.
[4] E. Mathieu, Memoire sur le mouvement vibratoire d'une membrance deforme elliptique, *Journal of Mathematique* 2 (13) (1868) 137–203.
[5] E. Mathieu, *Cours de Physique Mathematique*, Gauthier-Villars, Paris, 1873.
[6] N.W. McLachlan, *Theory and Applications of Mathieu Equations*, Oxford University Press, London, 1947.
[7] E.T. Whittaker, General solution of Mathieu's equation, *Proceedings of Edinburgh Mathematics Society* 32 (1913) 75–80.
[8] E.T. Whittaker, G.N. Watson, *A Course of Modern Analysis*, Cambridge University Press, London, 1935.
[9] H. Jeffreys, On certain solutions of Mathieu equation, *Proceedings of London Mathematics Society* 23 (1925) 437–448.
[10] E. Sevin, On the parametric excitation of pendulum-type vibration absorber, *American Society of Mechanical Engineers Journal of Applied Mechanics* 28 (1961) 330–334.
[11] C.S. Hsu, On the parametric excitation of a dynamics system having multiple degrees of freedom, *American Society of Mechanical Engineers Journal of Applied Mechanics* 30 (1963) 369–372.
[12] C.S. Hsu, Further results on parametric excitation of a dynamics system, *American Society of Mechanical Engineers Journal of Applied Mechanics* 32 (1965) 373–377.
[13] W.K. Tso, T.K. Caughey, Parametric excitation of a nonlinear system, *American Society of Mechanical Engineers Journal of Applied Mechanics* 32 (1965) 899–902.
[14] M. Mond, G. Cederbaum, P.B. Khan, Y. Zarmi, Stability analysis of non-linear Mathieu equation, *Journal of Sound and Vibration* 167 (1) (1993) 77–89.
[15] R.S. Zounes, R.H. Rand, Transition curves for the quasi-periodic Mathieu equations, *SIAM Journal of Applied Mathematics* 58 (4) (2000) 1094–1115.

[16] V.K. Melnikov, On the behavior of trajectories of system near to autonomous Hamiltonian systems, *Soviet Mathematics-Doklady* 3 (1962) 109–112.
[17] V.K. Melnikov, On the stability of the center for time periodic perturbations, *Transactions Moscow Mathematics Society* 12 (1963) 1–57.
[18] M. Henon, C. Heiles, The applicability of the third integral motion: some numerical experiments, *Astronomical Journal* 69 (1964) 73–79.
[19] D.F. Escande, F. Doveil, Renormalization method for the onset of the stochasticity in Hamiltonian systems, *Physics Letters A* 83 (1981) 307–310.
[20] D.F. Escande, Stochasticity in classic Hamiltonian systems: universal aspects, *Physics Report* 121 (1985) 165–261.
[21] A.J. Lichtenberg, M.A. Lieberman, *Regular and Chaotic Dynamics*, 2nd Edition, Springer, New York, 1992.
[22] A.C.J. Luo, Analytical Modeling of Bifurcations, Chaos and Fractals in Nonlinear Dynamics, Ph.D. Dissertation, University of Manitoba, Winnipeg, Canada, 1995.
[23] R.P.S. Han, A.C.J. Luo, Resonant layers in nonlinear dynamics, *American Society of Mechanical Engineers Journal of Applied Mechanics* 65 (1998) 727–736.
[24] A.C.J. Luo, R.P.S. Han, Analytical predictions of chaos in a nonlinear rod, *Journal of Sound and Vibration* 227 (3) (1999) 523–544.
[25] A.C.J. Luo, Resonant layers in a parametrically excited pendulum, *International Journal of Bifurcation and Chaos* 12 (2) (2002) 409–419.
[26] K. Feng, M.Z. Qin, Hamiltonian algorithms for Hamiltonian systems and a comparative numerical study, *Computational Physical Communication* 65 (1991) 173–187.
[27] R. McLachlan, P. Atela, The accuracy of symplectic integrators, *Nonlinearity* 5 (1992) 541–562.
[28] J.M. Greene, Two-dimensional measure-preserving mappings, *Journal of Mathematical Physics* 9 (1968) 760–768.
[29] J.M. Greene, A method for computing the stochastic transition, *Journal of Mathematical Physics* 20 (1979) 1183–1201.